Flexural vibration of an infinite wedge

Rajendra Gunda, Sandeep M. Vijayakar, and Rajendra Singh[a)]
Acoustics and Dynamics Laboratory, Department of Mechanical Engineering, The Ohio State University, 206 West 18th Avenue, Columbus, Ohio 43210-1107

(Received 17 July 1996; accepted for publication 23 January 1997)

A new solution to the problem of flexural vibration of an infinite wedge excited by a point harmonic load is obtained via a superposition of the geometric and diffraction fields, for simply supported and roller boundary conditions along the edges. The diffraction integrals are evaluated both in closed form in terms of the Faddeeva function and also as an asymptotic series using the steepest descent method. An eigensolution is also derived by expanding eigenfunctions in the angular direction and propagation terms in the radial direction. These two representations of the solution are compared numerically for accuracy and spatial distribution in different frequency regimes. The relative contribution of the geometric and diffraction fields to the overall solution is examined. This result is then compared to the second-order Helmholtz wave equation solution in order to demonstrate the near-field effects arising due to the fourth-order biharmonic formulation. The authors' motivation for obtaining the solution for a wedge-shaped infinite plate is that it is an essential step toward devising numerical models for the vibration of arbitrary polygonal plates. By combining the contribution from diffraction at the vertices of a polygonal plate with the geometrical solution obtained by the method of images, the authors expect to obtain better predictions at mid and high frequencies than is possible by other available methods. [S0001-4966(97)00406-2]

PACS numbers: 43.40.Dx, 43.40.At [CBB]

INTRODUCTION

The diffraction effects arising from wedge-shaped geometries are of interest in several disciplines including acoustics, optics, geophysics, and electromagnetics.[1–7] For those wedge angles β which are submultiples of π, any process of isotropic symmetry can be solved by applying the *method of images*.[8] This technique was generalized by Bromwich[2] for noninteger wedge indices by using a complex integral representation of the image series.[9] For instance, Bowman and Senior[4] have generated solutions for E and H polarized electric fields in noninteger wedges with various source excitations. The diffraction effects for the flexural vibration of thin wedge-shaped plates have not been analyzed before to the best of our knowledge. Previous investigations have been confined to phenomena governed by the classical wave equation, where as in plate vibrations a biharmonic formulation is required. In this article, the arbitrary structural wedge problem is formulated and the diffraction integral is evaluated in closed form by using an asymptotic expansion of Hankel functions for large arguments. The diffraction integral is also evaluated by the method of steepest descent, a high-frequency approximation, that is equivalent to the geometric theory of diffraction as introduced by Keller.[10]

The region enclosed by the wedge of Fig. 1 is given in cylindrical polar coordinates as

$$\mathbf{r} \equiv (\rho, \phi) \in [0, \infty) \times [0, \beta]. \tag{1}$$

The wedge index (ν) is defined in terms of wedge angle (β) as $\nu = \pi/\beta$. The thickness of the plate is denoted by h. Wedges are classified as integer wedges if ν is an integer and as noninteger wedges if ν is not an integer.

According to the classical thin plate theory,[11] the equation governing the flexural motion of an isotropic, homogeneous plate of constant thickness h is expressed in terms of transverse displacement $w(\mathbf{r},t)$ as

$$D\nabla^4 w(\mathbf{r},t) + \rho_m h \frac{\partial^2 w(\mathbf{r},t)}{\partial t^2} = p(\mathbf{r},t), \tag{2}$$

where $D = Eh^3/12(1-\nu^2)$ is the flexural rigidity of the plate; further, ∇^4, t, E, ρ_m, p, and ν are the biharmonic operator, time, Young's modulus, density, lateral force per unit area, and Poisson's ratio, respectively. For harmonic excitation at a frequency ω, $p(\mathbf{r},t) = F(\mathbf{r})\exp(-i\omega t)$, the response w is given by $w(\mathbf{r},t) = u(\mathbf{r})\exp(-i\omega t)$. From this point on, the analysis is carried out in spectral domain in terms of $u(\mathbf{r})$ and $F(\mathbf{r})$, and the $\exp(-i\omega t)$ time dependence is dropped from expressions for the sake of brevity. The governing equation is expressed in terms of the bending wave number γ as

$$(\nabla^4 - \gamma^4) u(\mathbf{r}) = F(\mathbf{r})/D, \quad \gamma^4 = \rho_m h \omega^2 / D. \tag{3}$$

Structural damping behavior is incorporated in the formulation by replacing D in Eq. (3) with $D = D(1 + i\eta)$ where η is the material loss factor. We consider a unit harmonic point load at the source point $S(\rho_s, \phi_s)$ as depicted in Fig. 1. The force distribution, for this case, is the Dirac delta function, $\delta(\mathbf{r} - \mathbf{r}_s)$.

a)Corresponding author.

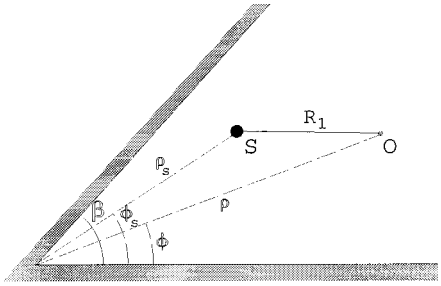

FIG. 1. The infinite wedge geometry with source at S, response or observation at O.

I. BOUNDARY CONDITIONS AND FUNDAMENTAL SOLUTION

In addition to satisfying the Eq. (3) inside the domain, the solution to the wedge vibration problem must satisfy certain boundary conditions. Assume that along the edges $\phi=0$ and $\phi=\beta$, either of the following conditions are satisfied.

$$\text{Simple supports:} \quad M_n(u)=0, \quad u=0,$$
$$\text{``Roller'':} \quad V_n(u)=0, \quad \frac{\partial u}{\partial \phi}=0. \tag{4}$$

Far away from the vertex along ρ, the Sommerfeld radiation or free-field condition must be satisfied, i.e., only outward propagating waves are assumed to exist:

$$\lim_{\rho\to\infty}\left\{\rho^{1/2}\left(\frac{\partial u}{\partial \rho}-i\gamma u\right)\right\}=0. \tag{5}$$

The fundamental solution to Eq. (3), $U(R(\phi-\phi_s);\gamma)$, represents the transverse deflection at a point $\mathbf{r}$ in an infinite plate due to a unit point load of frequency ω at $\mathbf{r}_s$. Let $R_1=R(\phi-\phi_s)=|\mathbf{r}-\mathbf{r}_s|$ be the distance between the source and observation points. The fundamental solution is given from[12,13] as

$$U(R(\phi-\phi_s);\gamma)=-\frac{i}{8\gamma^2 D}\,[H_0^{(1)}(\gamma R_1)-H_0^{(1)}(i\gamma R_1)], \tag{6}$$

where $H_0^{(1)}$ is the zeroth-order Hankel function of the first kind. Since we use the Hankel function of the first kind only, the superscript (1) is dropped from now on. For high-frequency excitation ($\gamma R_1\gg 1$), a simplified form of Eq. (6) is obtained by using an asymptotic expansion of Hankel functions for large argument:[14]

$$H_0(z)\approx\sqrt{\frac{2}{\pi z}}\exp\left\{i\left(z-\frac{\pi}{4}\right)\right\}, \quad -\pi<\arg(z)<2\pi. \tag{7}$$

Hence, the fundamental solution (6) is simplified for $\gamma R_1\gg 1$ as

$$\begin{aligned}U(R(\phi-\phi_s);\gamma)\approx&-\frac{i}{8\gamma^2 D}\sqrt{\frac{2}{\pi\gamma R_1}}\\&\times\left[\exp\left\{i\left(\gamma R_1-\frac{\pi}{4}\right)\right\}+i\,\exp(-\gamma R_1)\right]\\=&K_p\left[\exp\left\{i\left(\gamma R_1-\frac{\pi}{4}\right)\right\}\right]\\&+K_p[i\,\exp(-\gamma R_1)],\end{aligned} \tag{8}$$

where

$$K_p=-\frac{i}{8\gamma^2 D}\sqrt{\frac{2}{\pi\gamma R_1}}.$$

II. ARBITRARY WEDGES

A. Integer wedges

In Fig. 1, $S(\rho_s,\phi_s)$ is the location of the excitation point and $O(\rho,\phi)$ is the observation point. For an integer wedge index, the solution at O can be constructed using the method of images.[8,15] The solution has contributions from the source at S and $2\nu-1$ images suitably placed to ensure the boundary conditions are satisfied:

$$\begin{aligned}u(\mathbf{r})=&\sum_{m=0}^{\nu-1}U\left[R\left(\frac{2m\pi}{\nu}+\phi_s-\phi\right);\gamma\right]\\&\mp U\left[R\left(\frac{2m\pi}{\nu}-\phi_s-\phi\right);\gamma\right].\end{aligned} \tag{9}$$

Each term in the series represents an ''image'' seen at the observation point O. Each image simulates waves reflected from boundaries and represents a ray path connecting S and O. It should be noted that, in this particular case of integer wedges, all the images are visible at any observation point, irrespective of its location within the domain. In Eq. (9), the negative sign gives the solution for simply supported boundary conditions while the positive sign is the solution for roller boundary conditions, as defined earlier by Eq. (4).

B. Noninteger wedges

A function $R(s)$ representing the distance between the observation and source/image points as a function of their relative angular positions is given by $R(s)=\{\rho^2+\rho_s^2-2\rho\rho_s\cos(s)\}^{1/2}$. For real s, we take the positive square root of $R(s)$. In order to solve the arbitrary wedge problem, it is convenient to let the argument s of the function $R(s)$ to become complex valued.[2,15] For complex s, we need to stay on the branch of the square root which has a positive real part. If we want to evaluate the contour integrals in the s plane, the contours should not cross a branch cut that is appropriately defined. The location of the branch points is given by

$$s=2l\pi\pm iq$$
$$\text{where} \quad l=0,\pm 1,\pm 2,\ldots, \quad q=\cosh^{-1}\frac{\rho^2+\rho_s^2}{2\rho\rho_s}. \tag{10}$$

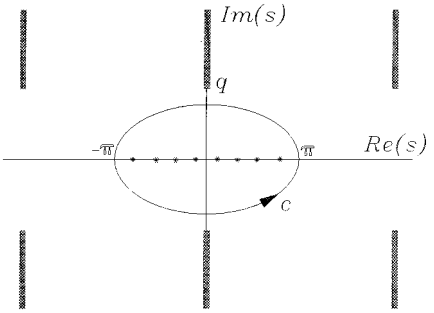

FIG. 2. Integration contour in s plane for integer ν. Poles of $h(s+\phi-\phi_s)$ and $h(s+\phi+\phi_s)$ are designated by an asterisk.

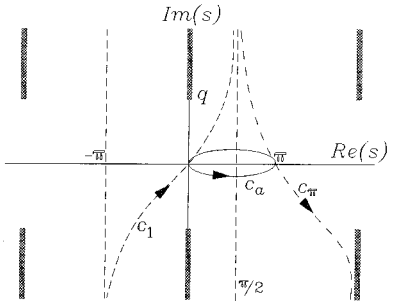

FIG. 3. Modified integration contour.

The branch cuts for $R(s)$ are vertical lines passing through the branch points and extending to $\pm\infty$. We like to replace Eq. (9) which is valid for integer ν by one of the form.

$$u(\mathbf{r})=\frac{1}{2\pi i}\oint_c U(R(s);\gamma)[h(s+\phi-\phi_s) \mp h(s+\phi+\phi_s)]ds. \tag{11}$$

The function $h(s)=\nu/2\cot(\nu s/2)$ is periodic in s with a period 2π, has poles at $s=2m\pi/\nu$ with a residue of unity at each pole. Note that $U(R(s);\gamma)$ has no poles in the s plane. The contour c is any simple loop which cuts the $\Re(s)$ axis at two points, 2π apart, as shown in Fig. 2. The representations for u as given by Eqs. (9) and (11) are equivalent from Cauchy's residue theorem. Thus, we have replaced Eq. (9) which is valid only for integer ν by Eq. (11) which holds for any ν.[2] Adjacent poles of $h(s)$ are $2\pi/\nu$ apart. Therefore, for integer ν, the contour c always encloses ν poles each of both $h(s+\phi-\phi_s)$ and $h(s+\phi+\phi_s)$. Hence, the solution given by Eq. (11) is continuous. For noninteger ν, the number of poles enclosed by the contour c is no longer fixed but varies depending on the location of the source and observation points. Hence, Eq. (11) gives a solution which is a discontinuous function of the position of the observation point. Therefore, the contour c has to be replaced by an equivalent contour which does not intersect the $\Re(s)$ axis. After a series of simplifications using contour deformations, symmetry and asymmetry properties of the integrand,[15] one arrives at the following representation for u:

$$u(\mathbf{r})=\frac{1}{2\pi i}\int_{c_1+c_a+c_\pi} U(R(s);\gamma)\sum h\, ds, \tag{12}$$

where

$$\sum h=[h(s+\phi-\phi_s)+h(s-\phi+\phi_s)] \mp[h(s+\phi+\phi_s)+h(s-\phi-\phi_s)]. \tag{13}$$

The contours c_1, c_a, and c_π are depicted in Fig. 3. The integral over c_1 is zero since c_1 is an inversion of itself and the integrand is odd. The integral over c_a is the geometric field and c_π is the diffracted field. The total field, at any point $u=u_g+u_d$ is composed of the geometric field u_g and diffraction field u_d. The poles of Σh occur when $\sin[(\pi/2\beta)(s\pm\phi\pm\phi_s)]$ vanishes or $s_p=2\beta l\pm\phi\pm\phi_s$. Only poles $0<s_p<\pi$ are enclosed by c_a and have to be taken into account when evaluating the geometric field. Therefore,

$$u_g(\mathbf{r})=\sum_l [U(R(2\beta l+\phi_s-\phi);\gamma) \mp U(R(2\beta l-\phi_s-\phi);\gamma)]. \tag{14}$$

The sum in Eq. (14) extends over all values of l for which the argument of R lies in the interval $(-\pi,\pi)$ corresponding to contributions of the images which are *visible* at the observation point.

III. THE DIFFRACTION INTEGRAL

The diffraction integral is evaluated by deforming the contour c_π to coincide with the line $\Re(s)=\pi$.

$$u_d(\mathbf{r})=\frac{1}{2\pi i}\int_{\pi+i\infty}^{\pi-i\infty} U(R(s);\gamma)\sum h\, ds. \tag{15}$$

Substituting $s=\pi-iz$ in Eq. (15) and simplifying gives

$$u_d(\mathbf{r})=\frac{-1}{4\beta}\int_{-\infty}^{\infty} U(R(\pi-iz);\gamma)[B_\nu(z,\phi-\phi_s) \mp B_\nu(z,\phi+\phi_s)]\, dz, \tag{16}$$

where

$$B_\nu(z,\phi)=\frac{-2\sin\nu\pi[(\cos\nu\pi-\cos\nu\phi)-(\cosh\nu z-1)\cos\nu\phi]}{(\cosh\nu z-1)^2+2(\cosh\nu z-1)(1-\cos\nu\pi\cos\nu\phi)+(\cos\nu\pi-\cos\nu\phi)^2}. \tag{17}$$

Equation (16) can be rewritten as

$$u_d(\mathbf{r}) = \frac{\sin\ \nu\pi}{2\beta} \int_{-\infty}^{\infty} U(R(\pi - iz);\gamma)[F_\nu(z,\phi-\phi_s) \mp F_\nu(z,\phi+\phi_s)]\ dz, \tag{18}$$

where

$$B_\nu(z,\phi) = -2\ \sin\ \nu\pi F_\nu(z,\phi). \tag{19}$$

Equation (18) explicitly shows the dependence of u_d on the wedge index ν. Hence for integer wedges, as expected, there is no diffraction field ($\sin\ \nu\pi = 0$) and the geometric field is the total solution. To find an approximate closed-form integral for Eq. (18), we need to study the behavior of the integrand for different values of z, as z goes from $-\infty$ to $+\infty$ along the $\Re(z)$ axis. Consider the part $F_\nu(z,\phi-\phi_s)$ and $F_\nu(z,\phi+\phi_s)$. Note that $F_\nu(z,\phi)$ has no singularities while z is on the real axis, as long as $z \neq 0$. If $z=0$, the denominator can become zero if $\cos\ \nu\pi = \cos\ \nu\phi$. Next examine $R(\pi - iz)$:

$$R(\pi - iz) = \{\rho^2 + \rho_s^2 + 2\rho\rho_s\ \cosh\ z\}^{1/2}. \tag{20}$$

Here, $R(\pi - iz)$ is positive and real for all $\Re(z)$ and has a minimum value at $z=0$. As z moves away from 0, along the real axis, $R(\pi - iz)$ stays real, but increases rapidly. This implies that the major contribution to the integral u_d comes from the region $z \approx 0$. Thus we may expand the integrand as a Taylor series around $z=0$ without losing much accuracy:

$$R(\pi - iz) \approx L\left\{1 + \frac{\rho\rho_s z^2}{2L^2}\right\} \quad \text{where } L = (\rho + \rho_s). \tag{21}$$

Now consider the $F_\nu(z,\phi)$ terms. Using $\cosh z \approx 1 + z^2/2$ and neglecting z^4 terms in the denominator in comparison to z^2 terms, we get

$$F_\nu(z,\phi) \approx \frac{1}{2\nu\sqrt{1-\cos\ \nu\pi\ \cos\ \nu\phi}} \left\{\frac{2M_\nu(\phi)}{z^2 + M_\nu(\phi)}\right\} = \frac{1}{2\nu\sqrt{1-\cos\ \nu\pi\ \cos\ \nu\phi}} \left\{\frac{1}{M_\nu(\phi) + iz} + \frac{1}{M_\nu(\phi) - iz}\right\}, \tag{22}$$

where

$$M_\nu(\phi) = \frac{\cos\ \nu\pi - \cos\ \nu\phi}{\nu\sqrt{1-\cos\ \nu\pi\ \cos\ \nu\phi}}. \tag{23}$$

Let $\Gamma = \sqrt{\gamma\rho\rho_s/\pi L}$. Then $\gamma R(\pi - iz) = \gamma L + \pi\Gamma^2 z^2/2$. Equation (8) can be rewritten as

$$U(R(\pi - iz);\gamma) = K_p e^{i(\gamma L - \pi/4)} e^{i\pi\Gamma^2 z^2/2} + K_p i e^{-\gamma L} e^{-\pi\Gamma^2 z^2/2}. \tag{24}$$

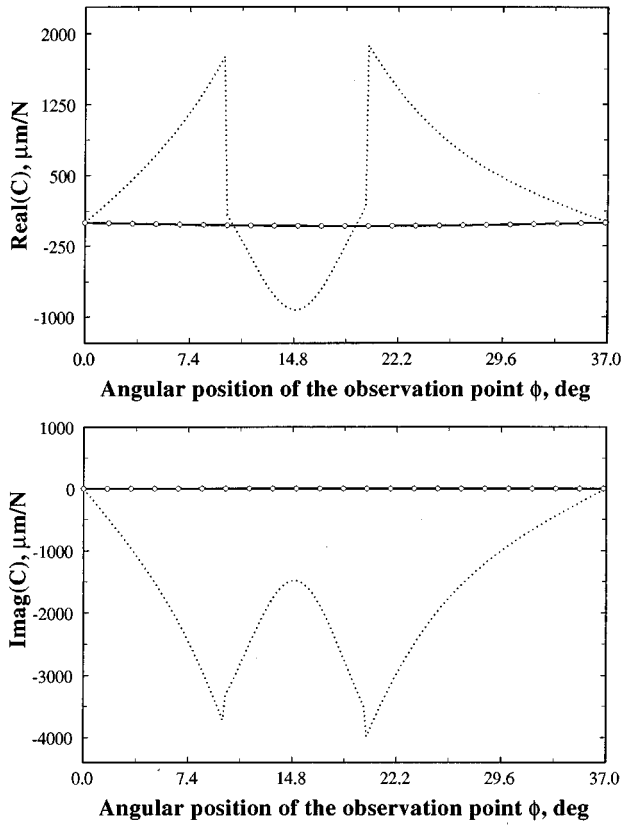

FIG. 4. Comparison of the closed-form solution with the eigenseries solution for $\gamma\rho\rho_s/2L = 0.1$ for simply supported boundary conditions along the edges. Key: ·····, $u_g(\mathbf{r}) + u_d(\mathbf{r})$; —○—, eigensolution.

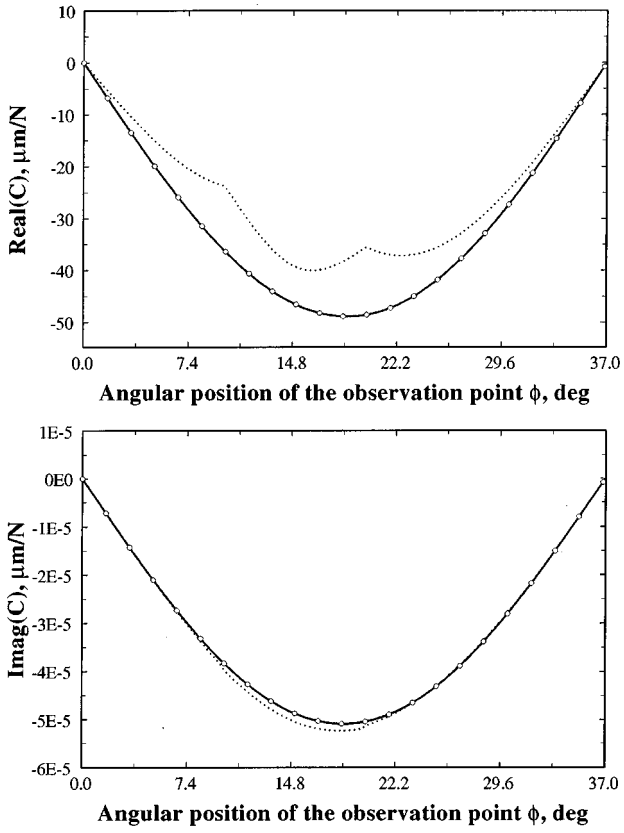

FIG. 5. Comparison of the closed-form solution with the eigenseries solution for $\gamma\rho\rho_s/2L = 1$ for simply supported boundary conditions along the edges. Key: ·····, $u_g(\mathbf{r}) + u_d(\mathbf{r})$; —○—, eigensolution.

An integral representation for the Faddeeva function $w(z) = \exp(-z^2)\mathrm{erfc}(-iz)$ is given by Eq. (25), where $\mathrm{erfc}(z)$ is the complementary error function:[16]

$$w(z) = \frac{i}{\pi}\int_{-\infty}^{\infty}\frac{\exp(-t^2)}{z-t}\,dt = \frac{i}{\pi}\int_{-\infty}^{\infty}\frac{\exp(-t^2)}{z+t}\,dt; \quad \Im(z)>0. \tag{25}$$

Let

$$V_{1\nu}(\phi) = \int_{-\infty}^{\infty}\frac{e^{i\pi\Gamma^2 z^2/2}}{M_\nu(\phi)-iz}\,dz = i\int_{-\infty}^{\infty}\frac{e^{-u^2}}{M_\nu(\phi)e^{i\pi/4}\sqrt{\pi/2}\Gamma+u}\,du = \pi\ \mathrm{sgn}(M_\nu(\phi))w\left(|M_\nu(\phi)|e^{i\pi/4}\sqrt{\frac{\pi}{2}}\,\Gamma\right). \tag{26}$$

Similarly,

$$V_{2\nu}(\phi) = \int_{-\infty}^{\infty}\frac{e^{-\pi\Gamma^2 z^2/2}}{M_\nu(\phi)-iz}\,dz = i\int_{-\infty}^{\infty}\frac{e^{-u^2}}{M_\nu(\phi)i\sqrt{\pi/2}\Gamma+u}\,du = \pi\ \mathrm{sgn}(M_\nu(\phi))w(i|M_\nu(\phi)|\sqrt{\pi/2}\Gamma). \tag{27}$$

Let

$$C_\nu(\phi) = K_p\{e^{i(\gamma L-\pi/4)}V_{1\nu}(\phi) + ie^{-\gamma L}V_{2\nu}(\phi)\}\frac{1}{\sqrt{1-\cos\ \nu\pi\ \cos\ \nu\phi}}. \tag{28}$$

Equation (18) is therefore written as

$$u_d(\mathbf{r}) = \frac{\sin\ \nu\pi}{2\pi}\,(C_\nu(\phi-\phi_s)\mp C_\nu(\phi+\phi_s)). \tag{29}$$

This is the closed-form representation for the diffraction field u_d, valid when $\gamma\rho\rho_s/2L \gg 1$. It can be deduced that $V_{2\nu}(\phi)$ is purely real from the fact that it is represented as a Faddeeva function of a purely imaginary argument and $w(z)$ satisfies the following property:[16] $w(z)=\overline{w(-\bar{z})}$.

IV. METHOD OF STEEPEST DESCENT

For high-frequency excitation, one can use uniform asymptotic expansions to reduce $V_{1\nu}(\phi)$ and $V_{2\nu}(\phi)$ into canonical forms, which are simpler to evaluate but contain the same essential features as the original integrals. This form of the solution may reveal certain features that are not quite evident in the closed-form integrals. Consider $V_{1\nu}(\phi)$:

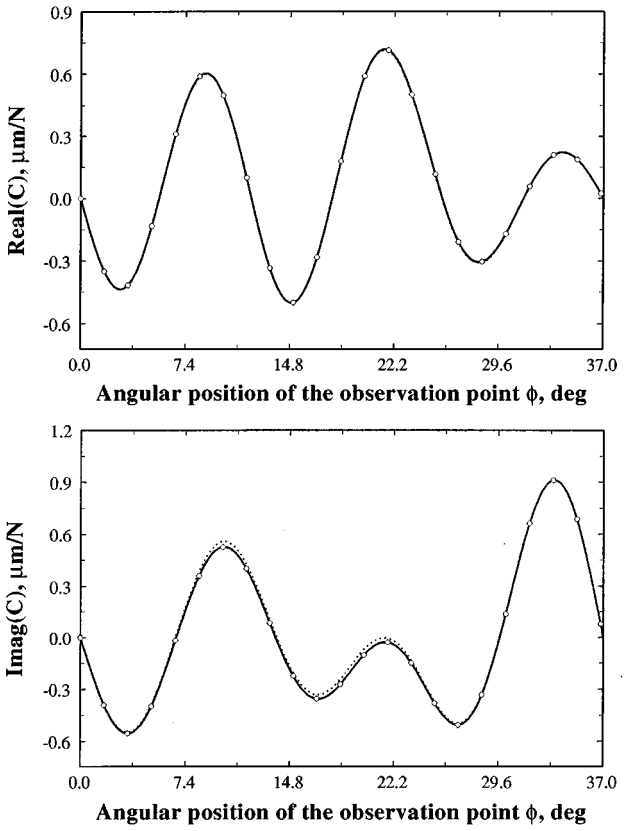

FIG. 6. Comparison of the closed-form solution with the eigenseries solution for $\gamma\rho\rho_s/2L=10$ for simply supported boundary conditions along the edges. Key: ·····, $u_g(\mathbf{r})+u_d(\mathbf{r})$; —○—, eigensolution.

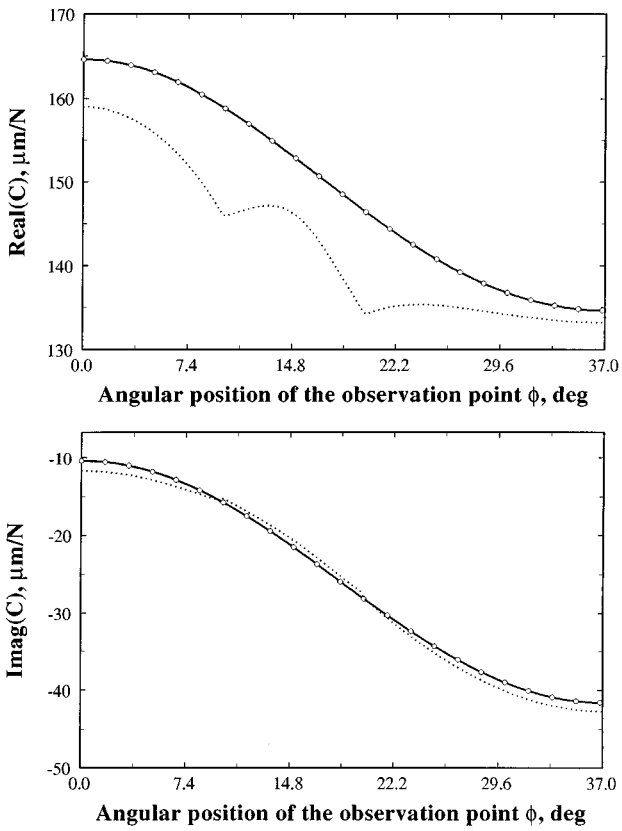

FIG. 7. Comparison of the closed-form solution with the eigenseries solution for $\gamma\rho\rho_s/2L=1$ for roller boundary condition along the edges. Key: ·····, $u_g(\mathbf{r})+u_d(\mathbf{r})$; —○——, eigensolution.

$$V_{1\nu}(\phi)=\int_{-\infty}^{\infty}\frac{e^{k(iz^2)}}{M_\nu(\phi)-iz}\,dz,\quad k=\pi\Gamma^2/2, \tag{30}$$

$z_s=0$ is the saddle point. On the steepest descent path through z_s, C_{sdp}, $|e^{k(iz^2)}|$ decreases most rapidly. This path makes an angle of $\pi/4$ with the $\Re(z)$ line. A variable transformation $\xi=ze^{-i\pi/4}$ causes C_{sdp} to coincide with the $\Re(\xi)$ line. Thus $V_{1\nu}(\phi)$ simplifies to

$$\begin{aligned}V_{1\nu}(\phi)&=\frac{1}{a}\int_{-\infty}^{\infty}\frac{e^{-k\xi^2}}{1-i\xi/a}\,d\xi,\\&=\frac{1}{a}\int_{-\infty}^{\infty}e^{-k\xi^2}\sum_{l=0}^{\infty}\left(\frac{i\xi}{a}\right)^l d\xi\\&=\frac{1}{a}\sum_{l=0}^{\infty}\int_{-\infty}^{\infty}e^{-k\xi^2}\left(\frac{i\xi}{a}\right)^l d\xi\\&=\frac{1}{a}\sum_{l=0}^{\infty}\frac{(-1)^l\Gamma((2l+1)/2)}{k^{(2l+1)/2}a^{2l}}\quad\text{if } M_\nu(\phi)\neq 0,\\&\qquad a=M_\nu(\phi)e^{-i\pi/4}.\end{aligned} \tag{31}$$

Similarly consider $V_{2\nu}(\phi)$:

$$V_{2\nu}(\phi)=\int_{-\infty}^{\infty}\frac{e^{-kz^2}}{M_\nu(\phi)-iz}\,dz. \tag{32}$$

The path of integration, $\Re(z)$ line, is the steepest descent path. Hence, no contour deformations are required. The integral for $V_{2\nu}(\phi)$ can be evaluated directly as

$$V_{2\nu}(\phi)=\frac{1}{b}\sum_{l=0}^{\infty}\frac{(-1)^l\Gamma((2l+1)/2)}{k^{(2l+1)/2}b^{2l}}$$
$$\text{if } M_\nu(\phi)\neq 0,\ b=M_\nu(\phi). \tag{33}$$

From the expressions (31) and (33), it is observed that, as the excitation frequency increases, $V_{1\nu}(\phi)$ and $V_{2\nu}(\phi)$ decrease due to the frequency related term k in the denominator, showing explicitly that diffraction is a low-frequency phenomenon. At high frequencies, the total solution is adequately represented by the geometric solution alone.

V. EIGENSERIES EXPANSION

Eigenseries representation for $u(\mathbf{r})$ is derived using eigenfunctions in the angular direction and propagation terms along the radial coordinate. This technique is similar to Macdonald's approach[17] for solving the Helmholtz equation in a wedge for a line source:

$$(\nabla^4-\gamma^4)u(\mathbf{r})=\frac{\delta(\rho-\rho_s)\,\delta(\phi-\phi_s)}{\rho D}. \tag{34}$$

Let us consider the simply supported boundary conditions first. Assume a solution of the form

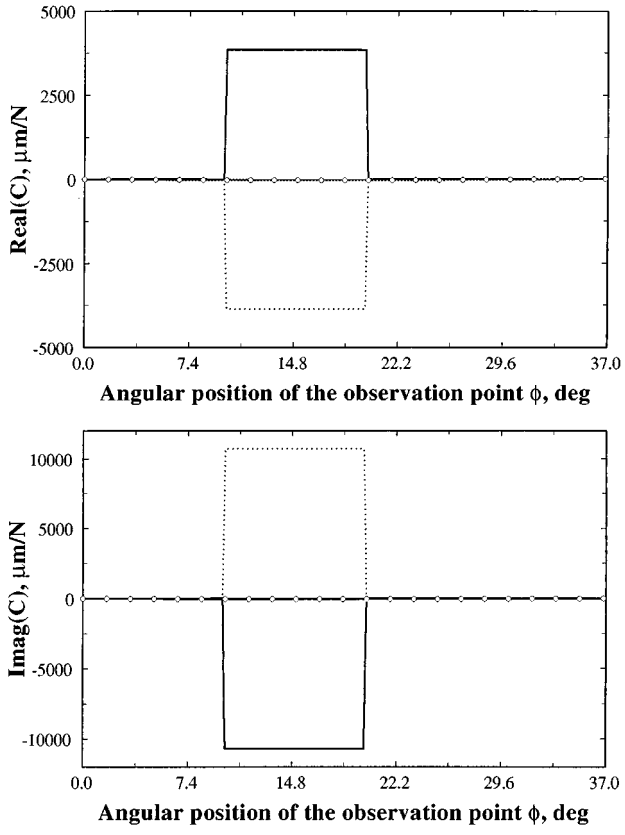

FIG. 8. Comparison of the geometric field with diffraction field for $\gamma\rho\rho_s/2L=0.1$ for simply supported boundary conditions along the edges. Key: ———, $u_g(\mathbf{r})$; ·····, $u_d(\mathbf{r})$; —○—, $u(\mathbf{r})$.

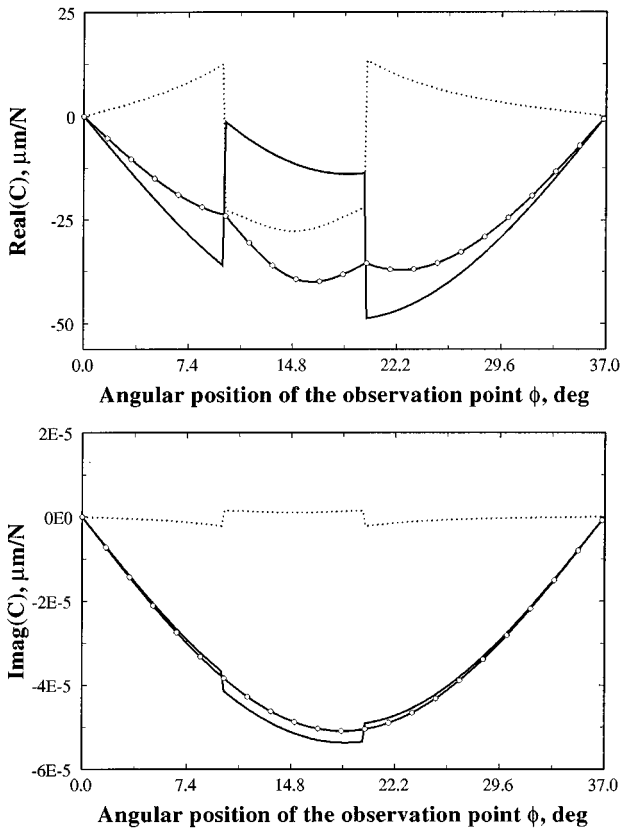

FIG. 9. Comparison of the geometric field with diffraction field for $\gamma\rho\rho_s/2L=1$ for simply supported boundary conditions along the edges. Key: ———, $u_g(\mathbf{r})$; ·····, $u_d(\mathbf{r})$; —○—, $u(\mathbf{r})$.

$$u(\mathbf{r})=\sum_{n=1}^{\infty} R_n(\rho)\sin(n\nu\phi). \tag{35}$$

Substituting Eq. (35) in Eq. (34), we get

$$\sum_{n=1}^{\infty} (\nabla^4-\gamma^4)R_n(\rho)\sin(n\nu\phi)=\frac{\delta(\rho-\rho_s)\delta(\phi-\phi_s)}{\rho D}. \tag{36}$$

Utilizing the orthogonality of the angular eigenfunctions, the radial solution $R_n(\rho)$ is obtained as

$$\begin{aligned} R_n(\rho)&=A_nJ_{n\nu}(\gamma\rho)+B_nH_{n\nu}(\gamma\rho)+C_nJ_{n\nu}(i\gamma\rho)\\ &\quad+D_nH_{n\nu}(i\gamma\rho), \quad \rho<\rho_s\\ &=W_nJ_{n\nu}(\gamma\rho)+X_nH_{n\nu}(\gamma\rho)+P_nJ_{n\nu}(i\gamma\rho)\\ &\quad+Q_nH_{n\nu}(i\gamma\rho), \quad \rho>\rho_s. \end{aligned} \tag{37}$$

The solution $u(\mathbf{r})$ satisfies zero displacement at the origin and the radiation condition at infinity, reducing the number of undetermined coefficients from eight to four.

$$\begin{aligned} R_n(\rho)&=A_nJ_{n\nu}(\gamma\rho)+C_nJ_{n\nu}(i\gamma\rho), \quad \rho<\rho_s\\ &=P_nH_{n\nu}(\gamma\rho)+Q_nH_{n\nu}(i\gamma\rho), \quad \rho>\rho_s. \end{aligned} \tag{38}$$

Across $\rho=\rho_s$, the displacement, slope, and bending moment are continuous. Matching the solutions at $\rho=\rho_s^-$ for displacement, slope, and bending moment with the corresponding quantities at $\rho=\rho_s^+$ results in the following relations between the coefficients. In Eq. (39), the prime stands for differentiation with respect to the variable ρ'.

$$\begin{bmatrix} J_{n\nu}(\gamma\rho_s) & J_{n\nu}(i\gamma\rho_s) & -H_{n\nu}(\gamma\rho_s) & -H_{n\nu}(i\gamma\rho_s)\\ J'_{n\nu}(\gamma\rho_s) & J'_{n\nu}(i\gamma\rho_s) & -H'_{n\nu}(\gamma\rho_s) & -H'_{n\nu}(i\gamma\rho_s)\\ J''_{n\nu}(\gamma\rho_s) & J''_{n\nu}(i\gamma\rho_s) & -H''_{n\nu}(\gamma\rho_s) & -H''_{n\nu}(i\gamma\rho_s) \end{bmatrix} \times \begin{Bmatrix} A_n\\ C_n\\ P_n\\ Q_n \end{Bmatrix} = \begin{Bmatrix} 0\\ 0\\ 0\\ 0 \end{Bmatrix}. \tag{39}$$

By using the following Wronskians of Bessel functions:[14]

$$\mathscr{W}(J_\nu(z),H_\nu(z))=\frac{2i}{\pi z},$$

$$J_\nu(z)H''_\nu(z)-J''_\nu(z)H_\nu(z)=\mathscr{W}(J_\nu(z),H_\nu(z))'=\frac{-2i}{\pi z^2}, \tag{40}$$

we find the solution to Eq. (39) as

$$\begin{Bmatrix} A_n\\ C_n\\ F_n\\ H_n \end{Bmatrix} = E_n \begin{Bmatrix} H_{n\nu}(\gamma\rho_s)\\ -H_{n\nu}(i\gamma\rho_s)\\ J_{n\nu}(\gamma\rho_s)\\ -J_{n\nu}(i\gamma\rho_s) \end{Bmatrix}. \tag{41}$$

Thus we are left with one undetermined coefficient, E_n, which is calculated by equating the transverse radial shear

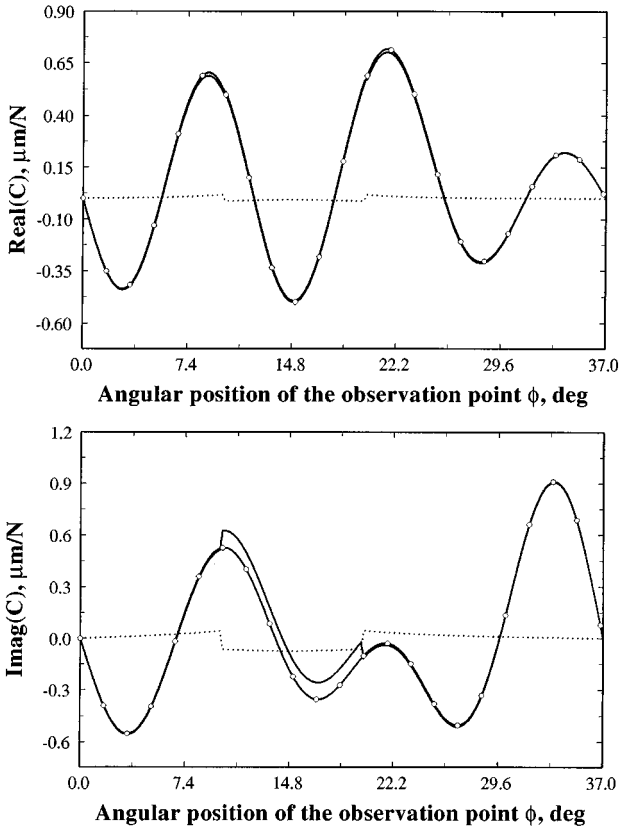

FIG. 10. Comparison of the geometric field with diffraction field for $\gamma\rho\rho_s/2L=10$ for simply supported boundary conditions along the edges. Key: ———, $u_g(\mathbf{r})$; ·····, $u_d(\mathbf{r})$; —○—, $u(\mathbf{r})$.

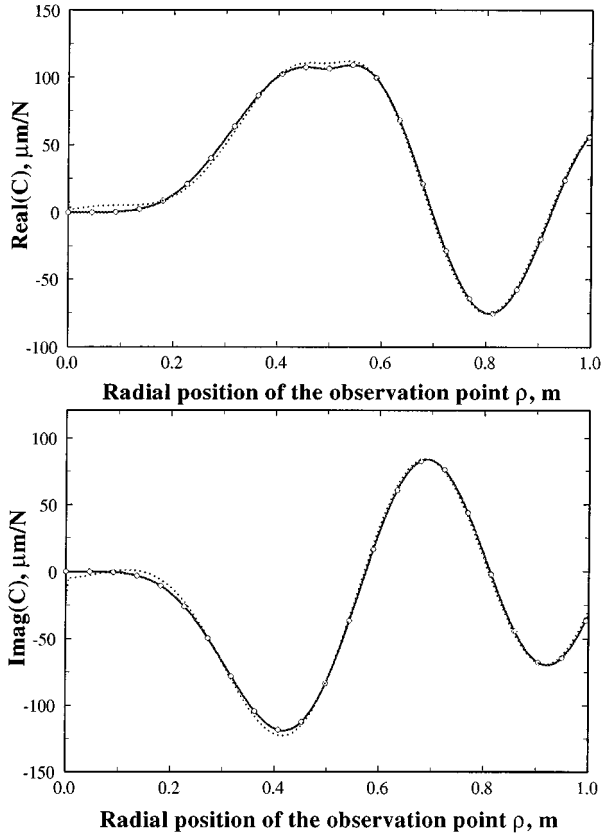

FIG. 11. Comparison of the closed-form solution with the eigenseries solution along a radial line for simply supported boundary conditions along the edges. Key: ·····, $u_g(\mathbf{r})+u_d(\mathbf{r})$; —○—, eigensolution.

force difference $V_r(\rho_s^+) - V_r(\rho_s^-)$ given by Eqs. (42) and (43) to the angular load distribution at ρ_s given in this case by $\delta(\phi - \phi_s)/\rho_s$:

$$V_r(\rho_s^+) = \gamma^2 D \sum_{n=1}^{\infty} E_n \sin n\nu\phi [J_{n\nu}(\gamma\rho_s) H'_{n\nu}(\gamma\rho_s) + J_{n\nu}(i\gamma\rho_s) H'_{n\nu}(i\gamma\rho_s)], \quad (42)$$

$$V_r(\rho_s^-) = \gamma^2 D \sum_{n=1}^{\infty} E_n \sin n\nu\phi [J'_{n\nu}(\gamma\rho_s) H_{n\nu}(\gamma\rho_s) + J'_{n\nu}(i\gamma\rho_s) H_{n\nu}(i\gamma\rho_s)]. \quad (43)$$

Here E_n is given by $-\nu i \epsilon_n \sin n\nu\phi_s / 4\gamma^2 D$. The complete expression for $u(\mathbf{r})$ for simply supported boundary conditions is given by

$$u(\mathbf{r}) = \frac{-\nu i}{4\gamma^2 D} \sum_{n=0}^{\infty} \epsilon_n \sin n\nu\phi \sin n\nu\phi_s \times \{J_{n\nu}(\gamma\rho^<) H_{n\nu}(\gamma\rho^>) - J_{n\nu}(i\gamma\rho^<) H_{n\nu}(i\gamma\rho^>)\}, \quad (44)$$

where

$$\rho^< \equiv \min(\rho, \rho_s), \quad \rho^> \equiv \max(\rho, \rho_s), \quad \epsilon_n = \begin{cases} 1, & n = 0 \\ 2, & n \geq 1. \end{cases} \quad (45)$$

Similarly, the solution for roller boundary conditions is given by

$$u(\mathbf{r}) = \frac{-\nu i}{4\gamma^2 D} \sum_{n=0}^{\infty} \epsilon_n \cos n\nu\phi \cos n\nu\phi_s \times \{J_{n\nu}(\gamma\rho^<) H_{n\nu}(\gamma\rho^>) - J_{n\nu}(i\gamma\rho^<) H_{n\nu}(i\gamma\rho^>)\}. \quad (46)$$

VI. RESULTS

In this section the relative contribution of the geometric $u_g(\mathbf{r})$ and the diffraction fields $u_d(\mathbf{r})$ to the overall solution $u(\mathbf{r})$ is examined at different frequencies. Also, their spatial properties along ρ and ϕ are studied using a specific example case for three different frequency regimes. Finally, the near-field effects, as induced by the biharmonic formulation, are examined.

A steel wedge with $\beta = 37°$, $E = 210$ GPa, $\rho_m = 7800$ kg/m^3, $\nu = 0.3$, and thickness of $h = 0.762$ mm is used as the primary example. The Faddeeva function is computed using the algorithm developed by Poppe and Wijers.[18] The force excitation point S is kept fixed at $\rho_s = 0.5$ m and $\phi_s = 22°$ and the angular position ϕ of the observation point O is varied between $[0, \beta]$ at a radial distance of $\rho = 0.3$ m. The closed-form solution $u_g(\mathbf{r}) + u_d(\mathbf{r})$ is compared with the eigensolution for $\gamma\rho\rho_s/2L = 0.1$, 1 and 10. The results are plotted in terms of the cross-point dynamic compliance spectrum $C(\omega; \mathbf{r}, \mathbf{r}_s) = u(\mathbf{r})/F(\mathbf{r}_s)$ over the range of interest as shown in Figs. 4–6 for the simply supported boundary conditions along the edges. Observe that the closed-form solu-

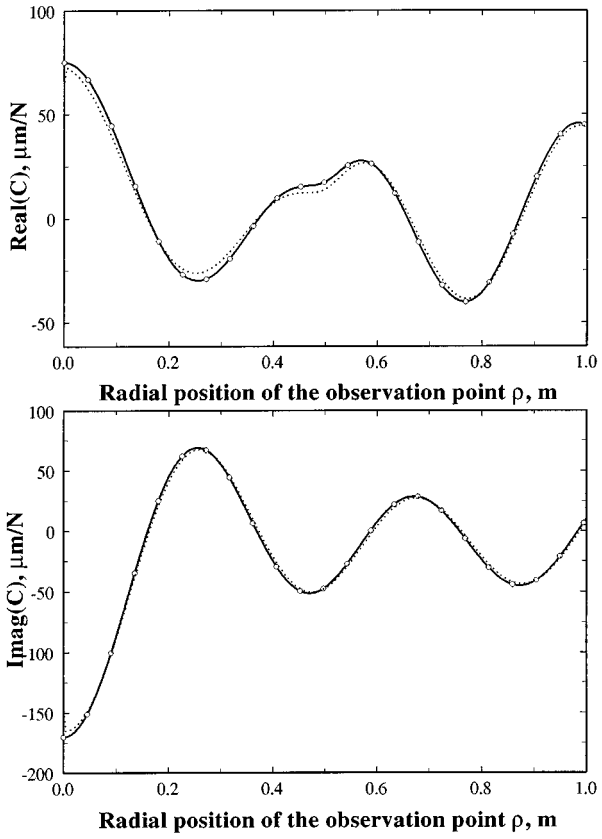

FIG. 12. Comparison of the closed-form solution with the eigenseries solution along a radial line for roller boundary conditions along the edges. Key: ·····, $u_g(\mathbf{r}) + u_d(\mathbf{r})$; —○—, eigensolution.

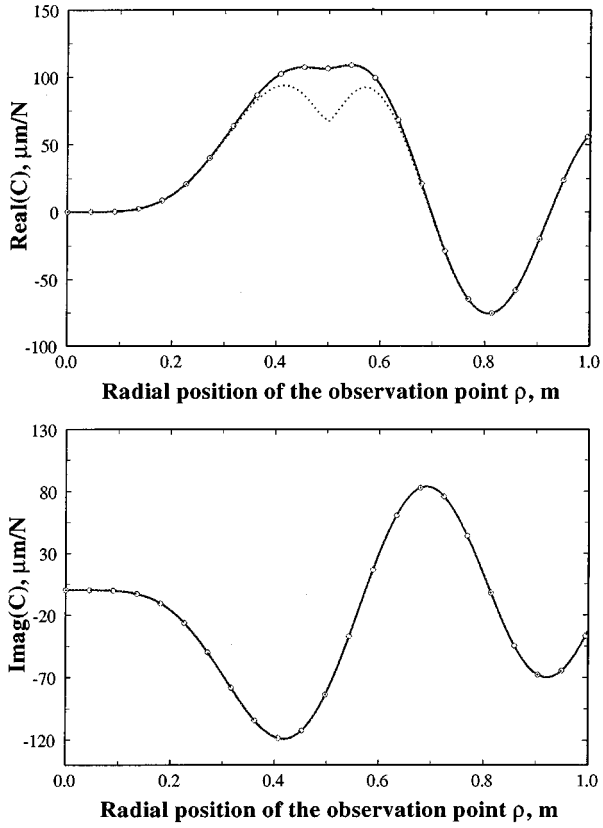

FIG. 13. Comparison of biharmonic solution with the classical wave equation solution along a radial line for simply supported boundary conditions along the edges. Key: —○—, biharmonic solution; ·····, classical wave equation solution.

tion is not very accurate for $\gamma\rho\rho_s/2L \leqslant O(0.1)$. It is expected since this was one of the assumptions involved in the derivation of the closed-form solution. Therefore, in order to calculate the the diffraction field $u_d(\mathbf{r})$ for small values of $\gamma\rho\rho_s/2L$, we must subtract the geometric field $u_g(\mathbf{r})$ from the total field $u(\mathbf{r})$ as given by the eigenseries expansion. Sample results for the roller boundary conditions along the edges are shown in Fig. 7 for $\gamma\rho\rho_s/2L=1$ from which similar conclusions can be drawn.

For the same example with simple supports, the geometric and the diffracted fields, $u_g(\mathbf{r})$ and $u_d(\mathbf{r})$ are plotted in Figs. 8–10. From these results, it is evident that the contribution of the diffraction field $u_d(\mathbf{r})$ to the total displacement field $u(\mathbf{r})$ is not as important as the geometric field $u_g(\mathbf{r})$ at higher frequencies as predicted by the steepest descent technique in Sec. IV. Therefore, we conclude that diffraction is basically a low-frequency phenomenon for the biharmonic problem, like the classical wave equation theory.[4,10] Next, the force excitation is located at $\rho_s=0.5$ m and $\phi_s=22°$ and the observation point is moved along a radial line at $\phi=18°$ from $\rho=0$ to $\rho=1$. Excellent agreement is seen between the closed-form solution and the eigensolution as evident from Fig. 11 (simply supported) and Fig. 12 (roller).

The first term of the fundamental solution (6) to the biharmonic equation satisfies the Helmholtz wave equation given by Eq. (47). By the ''Helmholtz wave equation solution,'' we refer to the solution of the following equation for the wedge geometry with Dirichlet or Neumann boundary conditions along the edges.[4]

$$(\nabla^2+\gamma^2)u(\mathbf{r})=\frac{1}{2\gamma^2 D}\,\delta(\mathbf{r}-\mathbf{r}_s). \tag{47}$$

Comparison of the fourth-order biharmonic with the second-order Helmholtz wave equation reveals that both yield similar solutions in most of the spatial domain except for small regions near the source and the boundary edges. This near-field effect is illustrated in Fig. 13.

VII. CONCLUSION

The chief contribution of this paper is the evaluation of the diffraction integral in a closed-form in terms of Faddeeva functions. Using the steepest descent method, it is analytically shown and numerically verified that the diffraction effects are important only at low frequencies. Near-field effects are significant only when the observation point is close to the edges or the excitation location. Finally, the eigenseries expansion converges rapidly at lower frequencies while $u_g(\mathbf{r})+u_d(\mathbf{r})$ predicts accurate high-frequency responses. Following the approach used in the derivation of eigenseries expansion, the solution to other excitations such as angularly distributed line load can be obtained. The solutions developed here will be used to address the problem of obtaining spectral characteristics of arbitrary finite polygonal plates with medium to high modal density for which there are no satisfactory techniques available at present. Future research will also examine other boundary conditions.

ACKNOWLEDGMENTS

This work has been supported by the U. S. Army Research Office (URI Grant No. DAAL-03-92-G-0120; Project Monitor: Dr. T. L. Doligalski).

[1] J. L. Graeme, *Geometric Theory of Diffraction for Electromagnetic Waves* (Institution of Electric Engineers, New York, 1986).
[2] T. J. I.'A. Bromwich, ''Diffraction of waves by a wedge, '' Proc. Math. Soc. London **14**, 450–463 (1915).
[3] A. A. Tuzhilin, ''New representations of diffraction fields in wedge-shaped regions with ideal boundaries,'' Sov. Phys. Acoust. **9**(2), 168–172 (1963).
[4] J. J. Bowman and T. B. A. Senior, ''The Wedge,'' in *Electromagnetic and Acoustic Scattering by Simple Shapes*, edited by J. J. Bowman, T. B. A. Senior, and P. L. E. Uslenghi (Hemisphere, New York, 1987), Chap. 6, pp. 252–283.
[5] F. J. W. Whipple, ''Diffraction by wedge and kindred problems,'' Proc. Math. Soc. London **16**, 481–500 (1915).
[6] M. A. Biot and I. Tolstoy, ''Formulation of wave propagation in infinite media by normal coordinates with an application to diffraction,'' J. Acoust. Soc. Am. **29**, 381–391 (1957).
[7] H. M. Macdonald, ''A class of diffraction problems,'' Proc. Math. Soc. London **14**, 410–427 (1915).
[8] A. Sommerfeld, *Partial Differential Equations in Physics* (Academic, New York, 1964).
[9] P. M. Morse and H. Feshbach, *Methods of Theoretical Physics* (McGraw-Hill, New York, 1953), Vol. 1.
[10] J. B. Keller, ''Geometrical theory of diffraction,'' J. Opt. Soc. Am. **52**(2), 116–130 (1961).
[11] A. W. Leissa, *Vibration of Plates* (NASA SP-160, NASA Special Publication, 1969).
[12] D. Feit and M. C. Junger, *Sound, Structures, and their Interaction* (MIT, Cambridge, MA, 1972), pp. 210–213.
[13] Y. Niwa, S. Kobayashi, and M. Kitahara, ''Eigen frequency analysis of a plate by the integral equation method,'' Theor. Appl. Mech. **29**, 287–367 (1981).
[14] G. N. Watson, *A Treatise on the Theory of Bessel Functions* (Cambridge U. P., Cambridge, England, 1944), pp. 196–200.
[15] A. D. Pierce, *Acoustics—An Introduction to its Physical Principles and Applications* (Acoustical Society of America, Woodbury, NY, 1989), pp. 481–500.
[16] M. Abramowitz and I. A. Stegun, *Handbook of Mathematical Functions with Formulas, Graphs, and Mathematical Tables* (Wiley, New York, 1972).
[17] H. M. Macdonald, *Electric Waves* (Cambridge U.P., Cambridge, England, 1902).
[18] G. P. M. Poppe and C. M. J. Wijers, ''Algorithm 680: Evaluation of the complex error function,''ACM Trans. Math. Softw. **16**(1), 47 (1990).